Journal of Power Sources 196 (2011) 1657–1664

Contents lists available at ScienceDirect

Journal of Power Sources

journal homepage: www.elsevier.com/locate/jpowsour

Efficient dye-sensitized solar cells with triarylamine organic dyes featuring functionalized-truxene unit

Mao Liang, Meng Lu, Qi-Lin Wang, Wei-Yi Chen, Hong-Yu Han, Zhe Sun, Song Xue*

Department of Applied Chemistry, Tianjin University of Technology, Tianjin 300384, PR China

ARTICLE INFO

Article history:
Received 22 April 2010
Received in revised form 19 August 2010
Accepted 23 August 2010
Available online 19 September 2010

Keywords:
Dye-sensitized solar cell
Photovoltaic performance
Truxene-based triarylamine
Dye aggregation
Dark current

ABSTRACT

Four triarylamine organic dyes featuring functionalized-truxene unit (**MXD1–4**) have been designed, synthesized, and characterized. It was found that these dyes favored light harvesting, prevented dye aggregation and suppressed the dark current significantly in dye-sensitized solar cells (DSSCs), leading to enhanced performance compared to the corresponding triphenylamine dye. As a result of retarding charge recombination benefiting from the steric hindrance of truxene units, high open circuit voltages (740–772 mV) were achieved based on the as-synthesized dyes. For a typical device a maximum power conversion efficiency of 6.04% was obtained under simulated AM 1.5 irradiation (100 mW cm^{-2}) with J_{sc} = 11.5 mA cm^{-2}, V_{oc} = 772 mV, and ff = 0.68.

1. Introduction

Dye-sensitized solar cells (DSSCs), developed by Grätzel and coworkers, have attracted considerable attention of many research groups in the past two decades owing to its high efficiency and low cost [1]. Conventional DSSCs typically contain four components: a mesoporous semiconductor metal oxide film; a sensitizer (dye); an electrolyte/hole transporter; and a counter electrode [2,3]. In these components, dye is one of the key components for high power conversion efficiencies. Attachment of sensitizers on the surface of the TiO_2 allows for efficient absorption of visible light and injects an electron into the conduction band of the TiO_2 after light excitation, generating the photocurrent. Actually, a lot of effort has been devoted to the synthesis and optimizing the dye component for DSSCs. At present, ruthenium dyes have achieved the maximum power conversion efficiencies of 11.4% in standard global air mass 1.5 and exhibited high stabilities [4]. However, they have encountered problems such as limited resources and elaborated purification [5]. In recent years, metal-free organic dyes were developed as an alternative to noble metal complexes for light harvesting owing to their high molar absorption coefficient, simple synthesis procedure and high efficiency. Various kinds of metal-free organic dyes with D-π-A structure such as coumarin [6], indoline [7], triphenylamine [8], dialkylaniline [9], bis(dimethylfluorenyl) aminophenyl [10], merocyanine [11], hemicyanine [12], and carbazole [13] have been investigated as sensitizers for DSSCs. And impressive device efficiencies of 9.7–10.3% have been achieved based on organic dyes [14,15]. However, it is still needed to optimize the chemical structures of organic dyes for further improvement on performances in the DSSCs.

The major factors for the low conversion efficiency of many organic dyes in the DSSCs are the dye aggregates on the semiconductor surface, which leads to self-quenching and reduces electron injection into TiO_2 [10b,16]. Introduction of a nonplanar architecture into the organic framework is a strategy to overcome the aggregation of dyes [17]. Recently, Ko et al. reported a novel triarylamine dye, **JK-1** [10a], containing nonplanar bis-dimethylfluorenyl unit. The DSSCs based on **JK-1** afforded a power conversion efficiency of 7.2%, which is higher than that of the corresponding triphenylamine dye. [18]. Their studies suggested that optimizing the triphenylamine moiety with steric architecture is a promising way for preventing unfavorable dye aggregation and increasing the stability of dye when exposed to light and high-temperature.

On the basis of the above considerations, a further improvement could be made by displacing phenyl unit with desirable candidates for constructing functionalized-triarylamine organic dyes. Truxene, recognized as a potential starting material for organic semiconductors, liquid crystalline compounds, and fullerene [19], is a promising candidate for this molecular design owing to its special properties as following: (1) bulky rigid conjugation structure; (2) facile introduction of alkyl chains; (3) outstanding thermal stability [20]. However, studies on truxene-based triarylamine organic dyes with D-π-A structure for application in DSSCs are very limited.

* Corresponding author. Tel.: +86 22 60214250; fax: +86 22 60214252.
E-mail address: xuesong@ustc.edu.cn (S. Xue).

0378-7753/$ – see front matter © 2010 Elsevier B.V. All rights reserved.
doi:10.1016/j.jpowsour.2010.08.055

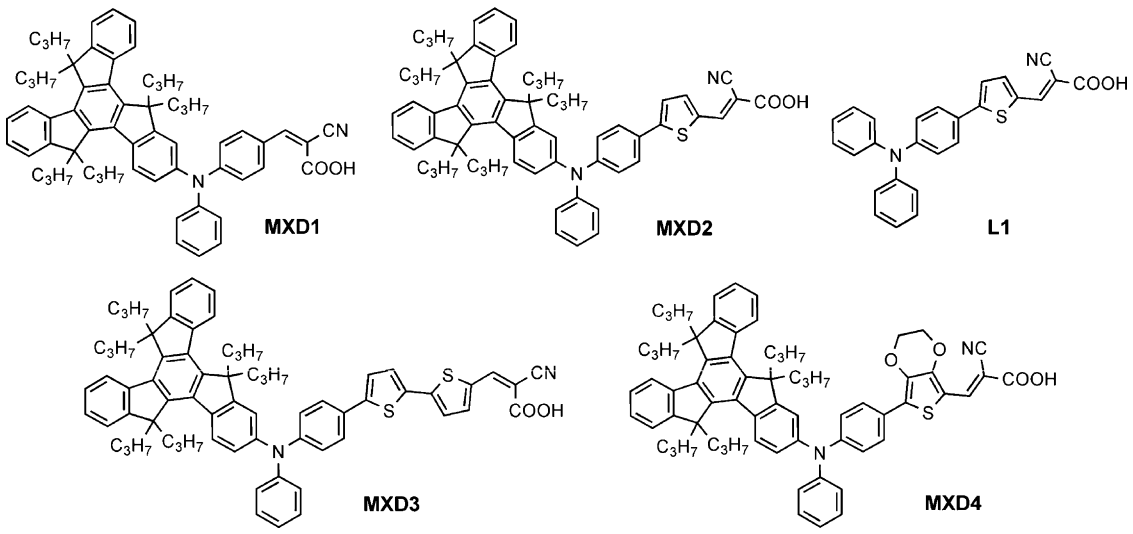

Scheme 1. Molecular structures of **MXD1–4** and **L1**.

We therefore designed and synthesized a new class of triarylamine organic dyes based on truxene (Scheme 1) that contain triarylamine as donor and cyanoacrylic acid as electron acceptor (anchoring groups), bridged by methine, thiophene, bithiophene or 3,4-ethylenedioxythiophene (EDOT), namely: **MXD1–4**. The n-propyl substituted truxene unit is introduced to the dyes to prevent dye aggregation, which will afford high power conversion. Herein, we report on the synthesis, characterization, and photovoltaic properties of the as-synthesized dyes. A triphenylamine dye employed one thiophene as linker, coded **L1** [18], is also synthesized for a comparison.

2. Results and discussion

2.1. UV–vis absorption/emission spectra

The absorption and emission of **MXD1–4** are listed in Table 1. Fig. 1a shows the UV/vis absorption spectra of the four dyes in dichloromethane. The four dyes display two strong absorption bands at around 300–380 nm and 400–600 nm, which mainly stem from the intramolecular charge-transfer transition. The maximum absorption of **MXD2** (486 nm) and **MXD3** (498 nm) were obviously red-shifted in comparison with that of **MXD1** (444 nm) owing to the expansion of conjugation systems by incorporating thiophene units. It is noted that **MXD4** (506 nm) bearing EDOT as electron linker shows a significant red shift (20 nm) in the long-wavelength band compared with that of **MXD2**, which may rise from the 3,4-ethylenedioxyl group enhancing the conjugated efficiency of EDOT and phenyl ring.

Table 1
Optical properties and electrochemical properties of four dyes.

Dye	λ_{max}/nm (ε/10^3 M^{-1} cm^{-1})[a]	λ_{max}/nm[b]	λ_{max}/nm[c]	λ_{int}/nm[d]
MXD1	320 (31), 444 (40)	579	343, 420	518
MXD2	350 (76), 486 (65)	613	353, 443	560
MXD3	360 (79), 498 (75)	637	364, 441	580
MXD4	360 (65), 506 (64)	622	360, 453	577

[a] Absorption spectra of dyes measured in CH_2Cl_2 with the concentrate of solution 1.0×10^{-5} M, ε is the extinction coefficient at λ_{max} of absorption.
[b] Emission spectra of dyes measured in CH_2Cl_2 with the concentrate of solution 1.0×10^{-5} M.
[c] Absorption spectra of dyes adsorbed on TiO_2.
[d] The intersect of the normalized absorption and the emission spectra.

Fig. 1b shows the UV/vis absorption spectrum of **L1** in THF. For comparison, the spectra of **MXD2** in THF and dichloromethane were also shown in Fig. 1b. Obviously, the **MXD2** in THF solution shows two strong absorptions while only one absorption band exhibits

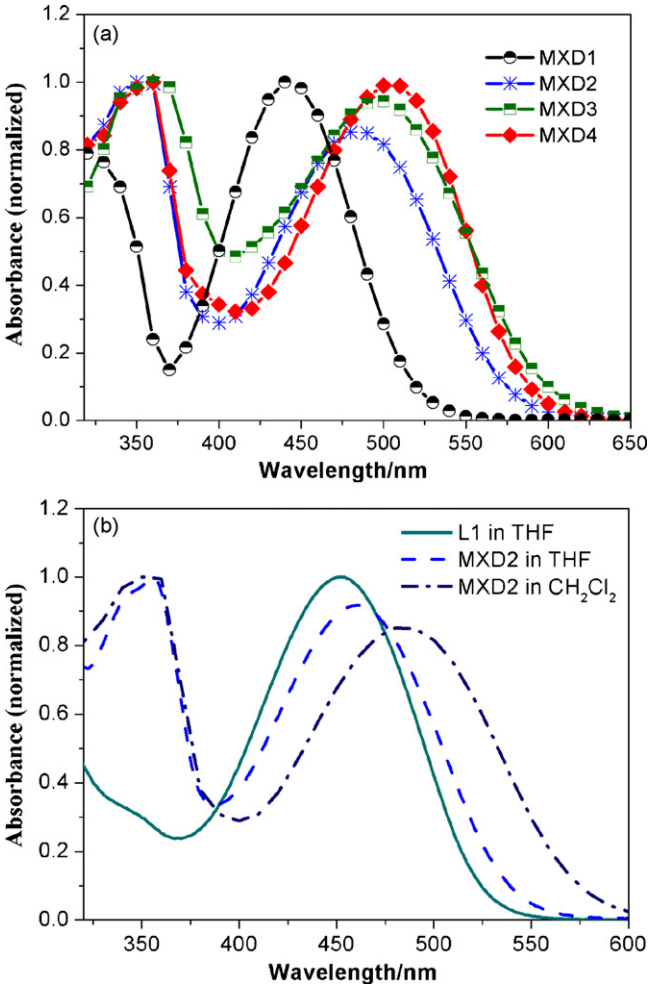

Fig. 1. (a) Absorption spectra of **MXD1–4** in dichloromethane with normalized absorbance. (b) Absorption spectra of **L1** in THF and **MXD2** in THF or dichloromethane with normalized absorbance.

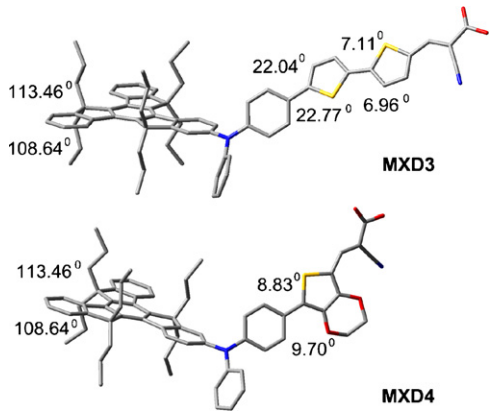

Fig. 2. Optimized geometrical configuration of **MXD3** and **MXD4**.

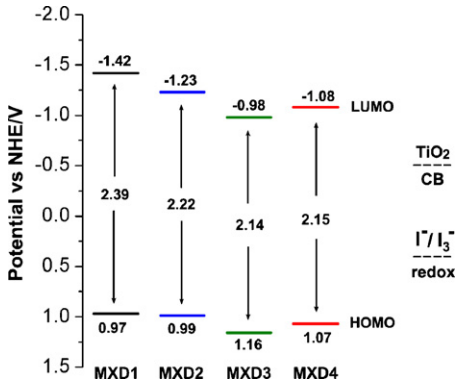

Fig. 4. Schematic energy levels of **MXD1–4** based on absorption and electrochemical data.

for **L1** in THF. Compared to **L1**, ca. 8 nm red-shift in the absorption peak together with increases in molar extinction coefficient (ε = 25 800 M^{-1} cm^{-1}, 453 nm, for **L1** in THF, ε = 64 000 M^{-1} cm^{-1}, 461 nm, for **MXD2** in THF) are found for **MXD2** dye. The broader spectral response and higher molar absorption coefficient imply that introduction of truxene unit into the dye favors light harvesting. The second absorption peak for **MXD2** in THF was red-shifted about 26 nm compared to that in dichloromethane solution, since high quantities of polar solvent decrease the electron-withdrawing power of the carboxylic acid [8g]. Moreover, the **MXD2** show a significant red shift (>55 nm) in visible absorption band compared with that of truxene-based dyes (**S5**–**S7**) reported by Ning et al. [21], indicating the position of truxene in the dye has an important effect on the behavior of absorption.

We have computed equilibrium structures for **MXD3** and **MXD4** dyes using density functional theory (DFT) at the B3LYP level (Fig. 2). Theoretical calculation shows that replacement of bithiophene with EDOT decreases the dihedral angle between phenyl and thiophenyl group ranging from 22.04°/22.77° to 8.83°/9.70°, thus resulting in a more planar conjugating system and therefore red shift of absorption band. The improved optical properties of **MXD4** dye suggest the merit of applying such electron-rich and highly planar linkers to sensitizer engineering [5]. In addition, the angle between propyl group and truxene ranges from 108.64° to 113.46°, forming a three-dimensional structure.

Fig. 3 shows the absorption spectra of **MXD1–4** anchored on transparent mesoporous TiO_2 films (3 μm), and the corresponding data are collected in Table 1. The maximum absorption peaks for **MXD1–4** are similar to the spectra of these dyes in dichloromethane, but exhibit a blue-shifted absorption compared to that in solution. Such a phenomenon was also found in other organic dyes, which may be ascribed to the formation of dye H-aggregates on the TiO_2 surface and/or the interaction between the dyes and TiO_2 [22]. The amounts of the dyes adsorbed on the TiO_2 surface were estimated spectroscopically by desorbing the dyes with a 0.01 M solution of KOH in methanol, and the surface concentrations were determined to be 0.73×10^{-7} mol cm^{-2} for **MXD1**, 0.80×10^{-7} mol cm^{-2} for **MXD2**, 0.76×10^{-7} mol cm^{-2} for **MXD3**, and 0.78×10^{-7} mol cm^{-2} for **MXD4**. The amounts of **L1** adsorbed on the TiO_2 surface was also estimated to be 1.25×10^{-7} mol cm^{-2} in the same conditions, small size of molecular leading to more dye-uptake.

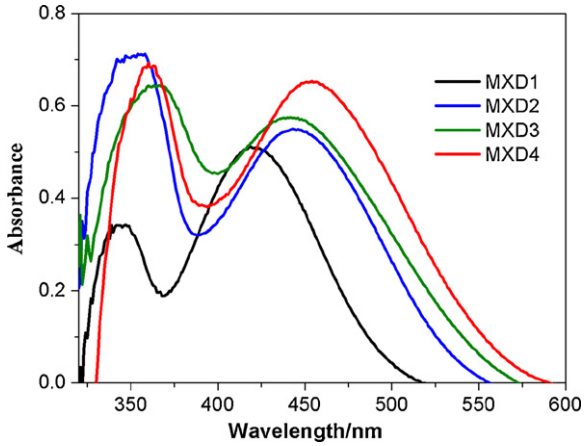

Fig. 3. Absorption spectra of the **MXD1–4** adsorbed on TiO_2 films.

Emission maxima of the four as-synthesized dyes can be found at 500–750 nm, respectively, when excited at their respective absorption bands at 400–600 nm. The corresponding data are also summarized in Table 1.

2.2. Electrochemical properties

The ground-state oxidation potential (E_{ox}) [8i] of as-synthesized dyes was determined from square-wave voltammograms under Ar atmosphere. The E_{ox} corresponds to the highest occupied molecular orbital (HOMO). The excited-state reduction potential (E_{red}) [8i], which corresponds to the lowest unoccupied molecular orbital (LUMO), can be calculated from E_{ox}–$E_{0\text{-}0}$ ($E_{0\text{-}0}$ values were calculated from λ_{int}: $E_{0\text{-}0} = 1240/\lambda_{int}$). As depicted in Fig. 4, extension the conjugation length by adding thiophene unit adjusts the HOMO and the LUMO level of these dyes. Positive shifts of the HOMO level (0.02 V) and the LUMO level (0.19 V) can be observed for **MXD2** vs **MXD1**, which narrows the HOMO and LUMO gaps. Also, this tendency holds for **MXD3** vs **MXD2** due to the extension of conjugation system through thiophene unit. EDOT unit has a stronger influence on the HOMO and LUMO level than that of thiophene unit, reflecting the strong electron-donating character of EDOT unit. The LUMO levels for these dyes (−0.98 to −1.42 eV) are more negative than the conduction band of TiO_2 (−0.5 V vs NHE), which provided sufficient driving forces for electron injection. On the other hand, the HOMO levels for these dyes (0.97–1.16 eV) are more positive than the iodine redox potential (0.4 V vs NHE) [23]. Thus, these oxidized dyes can be regenerated from the reduced species in the electrolyte to give an efficient charge separation.

2.3. Photovoltaic properties

The incident photon-to-current conversion efficiency (IPCE) of DSSCs based on **MXD1–4** are measured in the visible region (400–800 nm), as shown in Fig. 5. The onsets of the IPCE spectra for

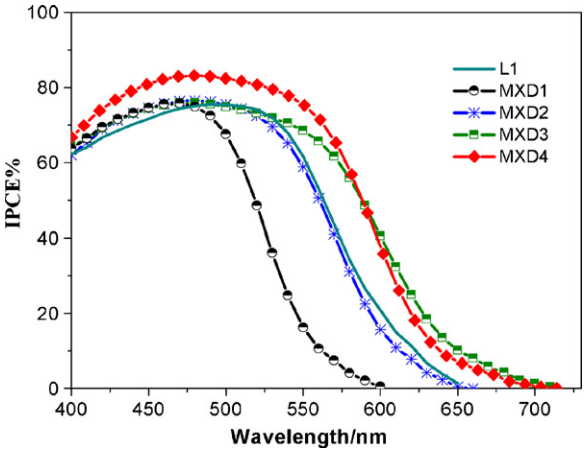

Fig. 5. IPCE spectra for DSSCs based on the **MXD1–4** and **L1** dyes.

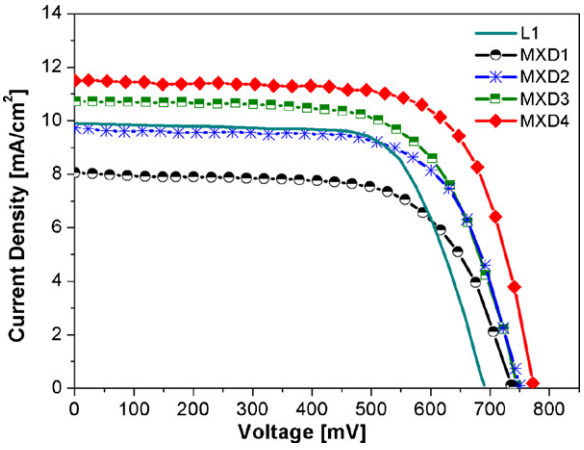

Fig. 6. Current–potential (*I–V*) curves for the DSSCs based on **MXD1–4** and **L1** under AM 1.5 irradiation (100 mW cm^{-2}).

the **MXD1–4**-based devices are significantly broadened and red-shifted compared to the absorption spectrum of the dyes absorbed on TiO_2 [24]. The IPCE spectrum for **MXD4** exhibits a high plateau from 440 to 530 nm where the incident photon-to-current conversion efficiency reaches 83% at 490 nm. As for **MXD3**, broader response of IPCE was obtained by increasing the linker conjugation with bithiophene. Among the four dyes, narrow response of IPCE was found for **MXD1**, showing the onset of the IPCE spectrum at 600 nm. The IPCE of **MXD4** is higher than that of **MXD1–3**, which might be due to good injection efficiency arising from EDOT unit. Interestingly, the IPCE action spectra of **MXD2** and **L1** are very similar, indicating similar capability of light harvesting and electron injection.

The photovoltaic properties of DSSCs based on **MXD1–4**, **L1** and **N719** are shown in Table 2 and photocurrent–voltage (*I–V*) curves for DSSCs based on the **MXD1–4** and **L1** are demonstrated in Fig. 6. **MXD4** sensitized cell gave a short-circuit photocurrent density (J_{sc}) of 11.5 mA cm^{-2}, an open-circuit voltage (V_{oc}) of 772 mV, and a fill factor (*ff*) of 0.68, corresponding to an overall conversion efficiency (η) of 6.04%. The power conversion efficiencies for **MXD3**, **MXD2**, and **MXD1** are 5.26%, 4.92%, and 3.89%, respectively. Clearly, relatively lower photocurrent of **MXD1** arises from narrower response of IPCE and results in lower photovoltaic performances. Under the same measuring conditions, the **N719**-sensitized cell showed an efficiency of 7.21% with a J_{sc} of 15.0 mA cm^{-2}, a V_{oc} of 740 mV, and a *ff* of 0.65. It is noted that the improved V_{oc} (740–772 mV) for DSSCs based on **MXD1–4** was achieved, which are even higher than that of **N719** (740 mV) in the same conditions. When the thiophene bridge is displaced by EDOT unit, a significantly high V_{oc} of 772 mV was achieved by **MXD4**.

L1 sensitized cell gave a short-circuit photocurrent density (J_{sc}) of 9.9 mA cm^{-2}, a V_{oc} of 690 mV, and a *ff* of 0.68, corresponding to an overall conversion efficiency of 4.64%. In contrast, an enhancement of open circuit voltage (750 mV) was obtained when **MXD2** dye was used as photosensitizer, leading to an increase of power conversion efficiency. In view of the amounts of dye on the TiO_2 surface, the adsorption amount of **L1** (1.25×10^{-7} mol cm^{-2}) is about 1.5-fold higher than that of **MXD2** dye (0.80×10^{-7} mol cm^{-2}), significantly higher IPCE for **L1** could be expected. However, the maximum IPCE of **L1** is just comparable to that of **MXD2**, which is mainly attributable to disadvantageous intermolecular energy transfer as a result of dye aggregate formation [5,25]. These results demonstrate that the presence of alkyl groups on truxene unit can suppress dye aggregation efficiently due to disturbance of the π–π stacking, which agrees with the previous research [13a,19].

To get a further explanation for the improvement in V_{oc} for DSSCs based on **MXD1–4**, measurement of the dark current–voltage characteristics is performed [21]. The dark current as a function of applied voltage is plotted in Fig. 7. The onset potentials of dark current (potential value at the dark current value of −0.1 mA cm^{-2}) for the **MXD1–4** and **L1** dyes are in the order of **L1** (490 mV) < **MXD1** (525 mV) < **MXD3** (547 mV) < **MXD2** (576 mV) < **MXD4** (585 mV), and the sequence is in accordance with that of the V_{oc} values. The onset voltages for dark current of **MXD1–4** are much higher than that of **L1**, which indicate that the dyes containing alkyl-functionalized truxene unit can reduce the interfacial electron recombination in the TiO_2 with the I^-/I_3^- redox couple in the electrolyte. The reduced election recombination process might be originated from the steric hindrance of truxene units. As shown in Fig. 8, the bulky structure of truxene blocks the I_3^- or cation approaching the TiO_2 surface, decreases the I_3^- con-

Table 2
Photovoltaic performance of DSSCs sensitized with **MXD1–4**, **L1** and **N719**[a].

Dye	J_{sc}/mA cm^{-2}	V_{oc}/mV	*ff*	η/%
MXD1	8.1	740	0.65	3.89
MXD2	9.8	750	0.67	4.92
MXD3	10.7	745	0.66	5.26
MXD4	11.5	772	0.68	6.04
L1	9.9	690	0.68	4.64
N719	15.0	740	0.65	7.21

[a] Photovoltaic performances of DSSCs based on **MXD1–4**, **L1** and **N719** were obtained without any coadsorption addition such as chenodeoxycholic acid, which is usually applied for preventing dye aggregation.

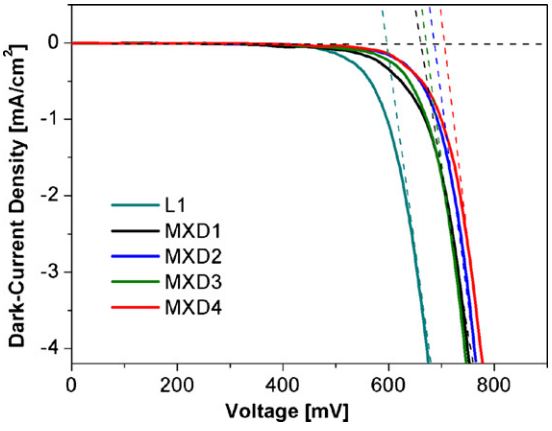

Fig. 7. Dark-current density–potential curves of DSSCs based on **MXD1–4** dyes and **L1**.

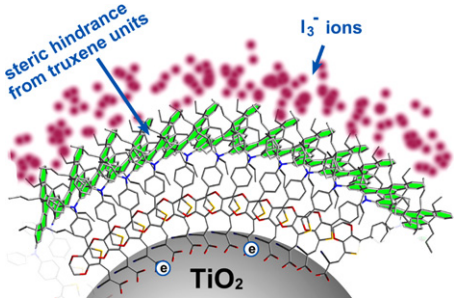

Fig. 8. Schematic representation of the bulky structure of truxene units, which blocking the I_3^- ions approaching the TiO_2 surface.

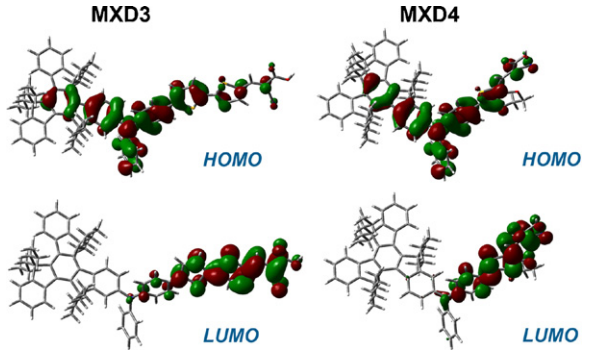

Fig. 9. The frontier molecular orbitals of the HOMO and LUMO calculated at B3LYP/6-31+G (D) level of **MXD3** and **MXD4**.

centration at the vicinity of the TiO_2, and increases the electron lifetimes. In addition, the propyl groups on **MXD1–4** dyes prefer to be oriented in uniform on the TiO_2 surface, which might retard the electron recombination process as well. It is evident that the respectable high V_{oc} values in DSSCs based on **MXD1–4** are obtained due to the alkyl-functionalized truxene unit which suppresses the dark current significantly.

2.4. Calculation analysis of dye structure

In order to obtain the geometrical configuration and characteristic features of the electronic structure of **MXD3** and **MXD4**, density functional theory (DFT) calculations were made on a B3LYP/6-31G level (Fig. 9). Obviously, the HOMO of the two sensitizers is delocalized over truxene-based triarylamine and bithiophene (or EDOT) moieties, and the LUMO is for both sensitizers delocalized across the bithiophene (or EDOT) and cyanoacrylic groups, indicating that the HOMO–LUMO excitation moves the electron distribution from the triarylamine to the cyanoacrylic acid moiety, thus allowing an efficient photoinduced electron transfer from the dye to the TiO_2 electrode under light irradiation. Also, these optimize geometrical configuration show uniform oriented alkyl chains on truxene units, favoring the molecular packing and arrangement of dyes on the TiO_2 surface.

3. Conclusions

In summary, we have designed and synthesized four new organic dyes (**MXD1–4**) featuring functionalized-triarylamine as the electron-donating moiety and cyanoacrylic acid as the electron acceptor. The noteworthy feature of these triarylamine dyes is introduction of alkyl-functionalized truxene unit into the electron donor moiety. The alkyl groups on the dyes enables to suppress the aggregation of dye molecules. The steric hindrance of truxene units reduces the dark current efficiently through blocking the I_3^- or cation approaching the TiO_2 surface, and improves photovoltaic performance compared to the corresponding triphenylamine dye. A cell based on the high molar extinction coefficient dye **MXD4** yields a maximum power conversion efficiency of 6.04% with J_{sc} = 11.5 mA cm^{-2}, V_{oc} = 772 mV, and *ff* = 0.68. These results demonstrate that optimizing the triphenylamine dye by introduction of functionalized-bulky groups with steric hindrance is effective in the development of DSSCs. The test of stability of DSSCs based on the as-synthesized dyes as well as further optimization of chemical structure of truxene-based triarylamine organic dyes will be done in our next work.

4. Experimental details

4.1. Materials and characterization

The synthetic routes of the four dyes are shown in Scheme 2. The starting material **1** was prepared by adopting literature procedures [26]. 5-Formylthiophen-2-ylboronic acid and n-butyllithium were purchased from Alfa. *N*,*N*-Dimethylformamide was dried over and distilled from CaH_2 under an atmosphere of nitrogen. Phosphorus oxychloride was freshly distilled before use. Dichloromethane and chloroform were distilled from calcium hydride under nitrogen atmosphere. Titanium(IV) isopropoxide, 1,3-dimethylimidazolium iodide, tertbutylpyridine and lithium iodide were purchased from Aldrich. All other solvents and chemicals used in this work were analytical grade and used without further purification.

^{1}H NMR and ^{13}C NMR spectra were recorded on a Bruker AM-300 or AM-400 spectrometer using $CDCl_3$ as solvent in all cases. The reported chemical shifts were against TMS. High resolution mass spectra were obtained with a Micromass GCT-TOF mass spectrometer.

4.2. Photophysical and electrochemical measurements

The absorption spectra of the dyes either in solution or on the adsorbed TiO_2 films was measured by HITACHI U-3310 spectrophotometer. Adsorption of the dye on the TiO_2 surface was done by soaking the TiO_2 electrode in a mixture solution ethanol–dichloromethane 3:1 solution of the dye (standard concentration 3×10^{-4} M) at room temperature for 24 h. Fluorescence measurement was carried with a HITACHI F-4500 fluorescence spectrophotometer.

Electrochemical measurements were performed at room temperature under Ar atmosphere on a Voltammetric Analyzer (Metrohm, μAutolab III) with polymer coated ITO glass as the working electrode, and platinum (Pt) plate as the counter electrode, using Ag/Ag$^+$ (nonaqueous) electrode as reference electrode with a scan rate of 50 mV s^{-1}. Tetrabutylammonium perchlorate (TBAP, 0.1 mol L^{-1}) and acetonitrile were used as supporting electrolyte and solvent, respectively. The measurements were calibrated using ferrocene as standard. The redox potential of ferrocene internal reference was taken as 0.63 V vs NHE. The solutions were purged with argon and stirred for 15 min before the measurements.

4.3. Fabrication of DSSCs

TiO_2 colloid was prepared according to the literature method [27], which was used for the preparation of the nanocrystalline films. The TiO_2 paste consisting of 18 wt.% TiO_2, 9 wt.% ethyl cellulose and 73 wt.% terpineol was firstly prepared, which was printed on a conducting glass (Nippon Sheet Glass, Hyogo, Japan, fluorine-doped SnO_2 over layer, sheet resistance of 10 Ω/sq) using a screen printing technique. The thickness of the TiO_2 film was controlled by selection of screen mesh size and repetition of printing. The film was dried in air at 120 °C for 30 min and calcined at 500 °C for

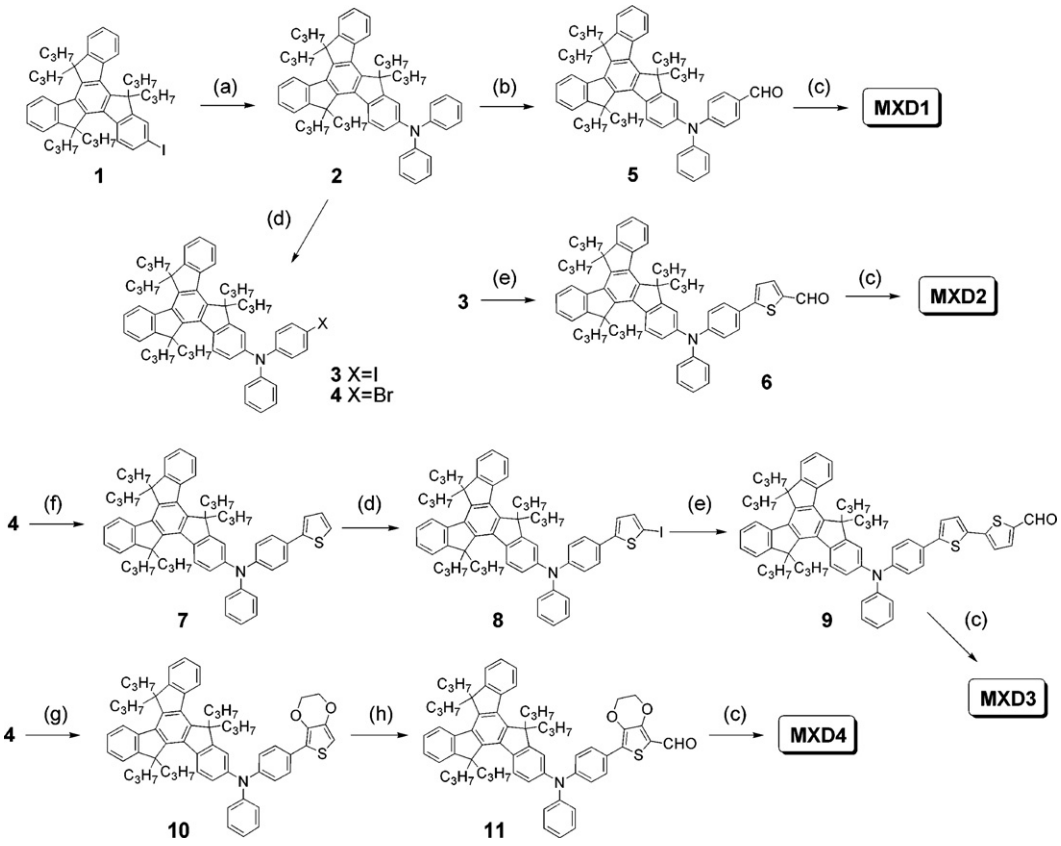

Scheme 2. Synthetic routes to the **MXD1**–**4** dyes. (a) Diphenylamine, Cu powder, 18-crown-6, K_2CO_3, 1,2-dichlorobenzene, reflux. (b) DMF/$POCl_3$, 100 °C. (c) $CNCH_2COOH$, NH_4OAc, AcOH, reflux. (d) NIS or NBS, $CHCl_3$. (e) 5-Formylthiophen-2-ylboronic acid, $Pd(PPh_3)_4$, Na_2CO_3, DME/H_2O, reflux. (f) Thiophen-2-ylboronic acid, $Pd(PPh_3)_4$, Na_2CO_3, DME/H_2O, reflux. (g) 2-(Tributylstannyl)-3,4-(ethelenedioxy)thiophene, $Pd(PPh_3)_4$, toluene, reflux. (h) DMF/$POCl_3$, rt.

30 min under flowing oxygen before cooling to room temperature. The heated electrodes were impregnated with a 0.05 M titanium tetrachloride solution in a water-saturated desiccator at 70 °C for 30 min and fired again to give a ca. 9 μm thick mesoscopic TiO_2 film. The TiO_2 electrode was stained by immersing it into a dye solution containing 300 μM dye sensitizers (ethanol for **MXD1** and **N719**, ethanol–dichloromethane 3:1 for **MXD2**–**4** and **L1**) for 48 h at room temperature. Then rinsed with dry ethanol and dried by a dry air flow. Pt catalyst was deposited on the FTO glass by coating with a drop of H_2PtCl_6 solution (40 mM in ethanol) with the heat treatment at 395 °C for 15 min to give photoanode. The dye-covered TiO_2 electrode and Pt-counter electrode were assembled into a sandwich type cell according to the literature method [27]. The DSSCs had an active area of 0.16 cm^2 and electrolyte composed of 0.6 M 1,2-dimethyl-3-n-propylimidazolium iodide (DMPImI), 0.1 M LiI, 0.05 M I_2, and 0.5 M tertbutylpyridine in acetonitrile.

4.4. Characterization of DSSCs

The photocurrent–voltage (*I*–*V*) characteristics of the solar cells were carried out using a Keithley 2400 digital source meter controlled by a computer and a standard AM1.5 solar simulator-Oriel 91160-1000 (300W) SOLAR SIMULATOR 2 × 2 BEAM. The light intensity was calibrated by an Oriel reference solar cell. The action spectra of monochromatic incident photon-to-current conversion efficiency (IPCE) for solar cell were performed by using a commercial setup (QTest Station 2000 IPCE Measurement System, CROWNTECH, USA).

4.5. Computational methods

Gaussian 03 package was used for Density functional theory (DFT) calculations [28]. We optimized the geometry of **MXD3** and **MXD4** using the B3LYP method with the 6-31+G(d) basis set. The stable geometry was confirmed by no imaginary frequency. Importantly, none of the frequency calculations generated negative frequencies, being consistent with an energy minimum for the optimized geometry.

4.6. The detailed experimental procedures and characterization data

The syntheses of **MXD1**–**4** are shown in Scheme 2. Iodide-substituted truxene **1** was used as starting material to react with diphenylamine in the presence of powdered anhydrous potassium carbonate, copper bronze, and 18-crown-6 to give key intermediate **2**. Aldehyde **5** was synthesized by Vilsmeier–Haack reaction of **2** with $POCl_3$ and DMF. Substituted triarylamine iodide **3** was cross-coupled with 5-formylthiophen-2-ylboronic acid under Suzuki conditions to give aldehyde **6**. Substituted triarylamine bromide **4** reacted with thiophen-2-ylboronic acid and 2-(tributylstannyl)-3,4-(ethelenedioxy)thiophene to gave intermediate **7** and **10**, respectively. Aldehyde **9** was prepared from **7** via iodonation reaction with NIS and Suzuki reaction with thiophen-2-ylboronic acid. The synthetic procedure for aldehyde **11** was similar to that for aldehyde **5** except that reacted at room temperature instead of 95 °C. Subsequently, the Knoevenagel condensation reactions of aldehydes **5**, **6**, **9** and **11** with cyanoacetic acid gave the target dyes.

*4.6.1. Triarylamine **2***

A stirred mixture of diphenylamine (1.16 g, 6.9 mmol), monosubstituted truxene iodide **1** (5 g, 6.9 mmol), powdered anhydrous potassium carbonate (4.76 g, 34.5 mmol), copper bronze (2.21 g, 34.5 mmol), and 18-crown-6 (120 mg) in 1,2-dichlorobenzene (80 mL) was refluxed for 20 h. After cooling, the solvent was removed under reduced pressure. The pure product **2** was obtained by silica gel chromatography (PE/DCM, 10/1) (3.69 g, 75%). ^{1}H NMR ($CDCl_3$, 300 MHz): δ 0.55–0.57 (m, 30H), 1.90–2.13 (m, 6H), 2.84 (m, 6H), 7.07–7.50 (m, 18H), 8.18 (d, J = 8.6 Hz, 1H), 8.31 (d, J = 7.4 Hz, 1H), 8.37 (d, J = 7.6 Hz, 1H). ^{13}C NMR ($CDCl_3$, 75 MHz): δ 14.6, 17.4, 36.3, 55.5, 117.6, 121.7, 122.3, 122.7, 124.3, 124.6, 125.3, 126.0, 126.3, 129.2, 135.1, 138.2, 140.3, 144.2, 144.8, 146.3, 147.9, 153.7, 155.1.

*4.6.2. Carbaldehyde **5***

1 g (1.31 mmol) of **2** was dissolved in 5 mL of DMF and Vilsmeyer reagent that was prepared from 5 mL of DMF and 1 g (6.55 mmol) of phosphorus oxychloride, and then the mixture was kept at 95 °C for 6 h. After neutralization with 25% NaOH solution to pH 8, the product was extracted by column chromatography (PE/EA, 10/1), resulting in carbaldehyde (**5**) (725 mg, 70%). ^{1}H NMR ($CDCl_3$, 300 MHz): δ 0.51–0.54 (m, 30H), 1.88–2.09 (m, 6H), 2.77–2.90 (m, 6H), 7.06–7.75 (m, 15H), 8.23 (d, J = 8.5 Hz, 2H), 8.26 (t, J = 7.8 Hz, 2H), 8.34 (d, J = 7.6 Hz, 1H), 9.85 (s, 1H). ^{13}C NMR ($CDCl_3$, 100 MHz): δ 14.5,17.3, 39.2, 55.6, 119.5, 119.8, 119.8, 122.3, 123.6, 124.6, 125.1, 126.1, 126.3, 126.5, 129.3, 129.7, 131.3, 137.2, 137.7, 138.3, 138.4, 140.1, 140.2, 144.5, 144.8, 144.9, 146.3, 153.4, 153.5, 155.5, 190.4. HRMS (ESI) calcd for $C_{58}H_{63}NO$ $[M+H]^+$: 790.4988. Found: 790.4996.

*4.6.3. **MXD1***

The carbaldehyde (**5**) (300 mg, 0.379 mmol), with cyanoacetic acid (42.5 mg, 0.5 mmol), ammonium acetate (87 mg, 1.13 mmol) and glacial acetic acid (10 mL) were mixed together and the solution heated to reflux for 6 h. After cooling to RT, the mixture was poured into a chilled aqueous solution to yield a red precipitate. It was filtered and thoroughly washed with water. The obtained red precipitate was then purified by column chromatography (DCM/methanol, 10:1) to afford **MXD1** (201.7 mg, 62%). ^{1}H NMR ($CDCl_3$, 300 MHz): δ 0.50 (m, 30H), 1.87–2.04 (m, 6H), 2.83 (m, 6H), 7.03–7.42 (m, 16H), 7.80 (m, 2H), 8.22–8.33 (m, 4H). ^{13}C NMR ($CDCl_3$, 75 MHz): δ 14.8, 18.3, 40.2, 56.3, 119.6, 120.2, 122.4, 123.6, 124.7, 125.6, 126.1, 126.4, 129.6, 132.9, 137.0, 137.6, 138.2, 140.0, 140.1, 144.3, 144.5, 144.6, 144.8, 146.1, 151.4, 153.4, 155.3. HRMS (ESI) calcd for $C_{61}H_{64}N_2O_2$ $[M+H]^+$: 857.5046. Found: 857.4971.

*4.6.4. Carbaldehyde **6***

N-Iodosuccinimide (236 mg, 1.05 mmol) was added to the **2** (800 mg, 1.05 mmol) in chloroform at temperature 0 °C and the mixture was stirred for 2 h in absence of light. After that, 20 mL of water was added into the flask, followed by extracted with dichloromethane, and the combined organic phase was dried over anhydrous sodium sulfate. After rotary evaporation of the solvent under a reduced pressure, crude **3** was obtained and used for the next step without any purification. Compound **3** (700 mg, 0.789 mmol), 5-formylthiophen-2-ylboronic acid (148 mg, 0.44 mmol), $Pd(PPh_3)_4$ (70 mg), and Na_2CO_3 (836 mg, 7.89 mmol) in 15 mL of DME and 3 mL of H_2O were heated to reflux under a nitrogen atmosphere for overnight. After cooling to room temperature, 20 mL of water was added into the flask, followed by extracted with dichloromethane, and the combined organic phase was dried over anhydrous sodium sulfate. The organic portion was combined and removed by rotary evaporation. The residue was purified by column chromatography with silica gel (PE/EA, 10/1) to yield **6** (467 mg, 68%). ^{1}H NMR ($CDCl_3$, 300 MHz): δ 0.50 (m, 30H), 1.92–2.06 (m, 6H), 2.86 (m, 6H), 7.12–7.28 (m, 4H), 7.31–7.39 (m, 3H), 7.41–7.49 (m, 8H), 7.50 (m, 2H), 7.63 (d, 2H), 7.75 (s, 1H), 8.24 (d, 1H), 8.31(d, 1H), 8.39 (d, 1H), 9.90 (s, 1H). ^{13}C NMR ($CDCl_3$, 100 MHz): δ 13.8, 17.4, 38.9, 55.5, 118.5, 122.3, 122.3, 122.6, 122.6, 122.9, 122.9, 124.6, 124.7, 125.1, 125.2, 125.4, 125.4, 126.0, 126.2, 126.3, 127.2, 129.5, 136.1, 137.6, 137.8, 137.9, 138.2, 138.3, 140.3, 141.3, 144.4, 144.5, 144.7, 145.3, 147.0, 149.2, 153.6, 154.6, 155.3, 182.5. HRMS (ESI) calcd for $C_{62}H_{65}NOS$ $[M+H]^+$: 872.4865. Found: 872.4879.

*4.6.5. **MXD2***

The synthesis method resembles that of **MXD1** (yield 73%). ^{1}H NMR ($CDCl_3$, 300 MHz): δ 0.50 (m, 30H), 1.88–2.04 (m, 6H), 2.83 (m, 6H), 7.05–7.68 (m, 19H), 8.19–8.34 (m, 4H). ^{13}C NMR ($CDCl_3$, 75 MHz): δ 14.8, 15.6, 40.1, 56.3, 118.5, 122.4, 122.6, 123.4, 123.9, 124.7, 125.2, 125.5, 126.1, 126.4, 127.4, 129.4, 134.3, 136.0, 137.8, 138.2, 140.0, 140.1, 140.2, 144.2, 144.4, 144.6, 145.2, 146.9, 148.7, 153.3, 155.1. HRMS (ESI) calcd for $C_{65}H_{66}N_2O_2S$ $[M+H]^+$: 939.4923. Found: 939.4892.

*4.6.6. Compound **7***

N-Bromosuccinimide (224 mg, 21 mmol) was added to the **2** (1 g, 1.31 mmol) in chloroform at room temperature and the mixture was stirred for 2 h. After that, 20 mL of water was added into the flask, followed by extracted with dichloromethane, and the combined organic phase was dried over anhydrous sodium sulfate. After rotary evaporation of the solvent under a reduced pressure, crude **4** was obtained and used for the next step without any purification. Crude **4** (800 mg, 0.95 mmol), thiophen-2-ylboronic acid (178 mg, 1.14 mmol), $Pd(PPh_3)_4$ (80 mg), and Na_2CO_3 (1.0 g, 9.5 mmol) in 15 mL of DME and 3 mL of H_2O were heated to reflux under a nitrogen atmosphere for overnight. After cooling to room temperature, 20 mL of water was added into the flask, followed by extracted with dichloromethane, and the combined organic phase was dried over anhydrous sodium sulfate. The organic portion was combined and removed by rotary evaporation. The residue was purified by column chromatography with silica gel (PE/DCM, 10/1), yield **7** (450 mg, 56%). ^{1}H NMR ($CDCl_3$, 400 MHz): δ 0.55 (m, 30H), 1.41–2.08 (m, 6H), 2.86 (m, 6H), 7.00–7.14 (m, 3H), 7.20–7.53 (m, 17H), 8.19 (d, J = 8.7 Hz, 1H), 8.26(d, J = 7.6 Hz, 1H), 8.35 (d, J = 7.8 Hz, 1H). ^{13}C NMR ($CDCl_3$, 100 MHz): δ 15.2, 18.4, 37.2, 56.4, 118.1, 121.9, 122.1, 122.4, 122.8, 123.2, 124.0, 124.3, 124.6, 124.7, 125.5, 126.1, 126.4, 126.8, 128.0, 128.8, 129.3, 135.5, 138.1, 138.3, 140.2, 140.3, 144.3, 144.7, 145.9, 147.2, 147.5, 147.9, 153.5, 155.1. HRMS (ESI) calcd for $C_{61}H_{65}NS$ $[M+H]^+$: 844.4916. Found: 844.4936.

*4.6.7. Carbaldehyde **9***

The synthesis method resembles that of compound **6** (yield 61%). ^{1}H NMR ($CDCl_3$, 400 MHz): δ 0.50–0.53 (m, 30H), 1.90–2.10 (m, 6H), 2.81 (m, 6H), 7.06–7.67 (m, 21H), 8.20 (d, J = 8.6 Hz, 1H), 8.29(d, J = 7.6 Hz, 1H), 8.36 (d, J = 7.4 Hz, 1H), 9.85 (s, 1H). ^{13}C NMR ($CDCl_3$, 100 MHz): δ 13.7, 17.3, 39.1, 55.5, 118.2, 122.3, 123.2, 123.3, 123.5, 123.7, 124.6, 124.6, 124.8, 125.4, 126.0, 126.3, 126.6, 127.1, 127.2, 129.4, 134.4, 135.7, 137.4, 137.9, 138.2, 138.2, 140.2, 141.3, 144.3, 144.4, 144.7, 145.6, 146.3, 147.3, 147.4, 148.1, 153.6, 155.3, 182.4. HRMS (ESI) calcd for $C_{66}H_{67}NOS_2$ $[M+H]^+$: 954.4742. Found: 954.4759.

*4.6.8. **MXD3***

The synthesis method resembles that of **MXD1** (yield 63%). ^{1}H NMR ($CDCl_3$, 300 MHz): δ 0.50 (m, 30H), 1.86–2.12 (m, 6H), 2.81 (m, 6H), 6.99–7.22 (m, 12H), 7.32–7.57 (m, 9H), 8.13–8.30 (m, 4H). ^{13}C NMR ($CDCl_3$, 75 MHz): δ 14.8, 18.3, 40.1, 56.2, 118.2, 122.3, 123.3, 124.7, 124.9, 125.4, 126.0, 126.6, 127.2, 129.4, 134.0, 135.6, 137.8, 138.1, 140.1, 140.2, 144.2, 144.6, 145.4, 147.1, 153.3, 155.0.

HRMS (ESI) calcd for $C_{69}H_{68}N_2O_2S_2$ $[M+H]^+$: 1021.4800. Found: 1021.4781.

4.6.9. Compound **10**

2-(Tributylstannyl)-3,4-(ethelenedioxy)thiophene (410 mg, 0.95 mmol), **4** (800 mg, 0.95 mmol), and $Pd(PPh_3)_4$ (80 mg) were dissolved in toluene (20 mL), and the reaction was refluxed under Ar for 6 h. After cooling down to room temperature, the mixture was poured into water and extracted with dichloromethane. The combined organic layer dried over anhydrous sodium sulfate. After rotary evaporation of the solvent under a reduced pressure, the residue was purified on a silica gel column (PE/DCM, 2/1) to give a yellow solid **10** (584 mg, 68%). ^{1}H NMR ($CDCl_3$, 400 MHz): δ 0.49 (m, 30H), 1.93–2.13 (m, 6H), 2.85 (m, 6H), 4.22–4.34 (m, 4H), 7.07–7.68 (m, 18H), 8.18 (d, J = 8.5 Hz, 1H), 8.31(d, J = 7.4 Hz, 1H), 8.39 (d, J = 7.7 Hz, 1H). ^{13}C NMR ($CDCl_3$, 100 MHz): δ 14.4, 17.3, 39.1, 55.5, 64.5, 64.7, 117.5, 117.8, 121.9, 122.3, 123.8, 124.0, 124.3, 124.6, 125.3, 125.9, 126.2, 126.8, 127.5, 129.2, 135.2, 137.5, 138.1, 138.1, 140.3, 140.4, 142.2, 144.2, 144.3, 144.8, 146.0, 146.3, 147.7, 153.6, 155.1. HRMS (ESI) calcd for $C_{63}H_{67}NO_2S$ $[M+H]^+$: 902.4971. Found: 902.4927.

4.6.10. ***MXD4***

The synthesis method resembles that of **MXD1** (yield 69%). ^{1}H NMR ($CDCl_3$, 300 MHz): δ 0.50 (m, 30H), 1.88–2.04 (m, 6H), 2.83 (m, 6H), 4.30–4.42 (m, 4H), 6.95–7.31 (m, 9H), 7.40–7.59 (m, 9H), 8.16–8.31 (m, 3H). ^{13}C NMR ($CDCl_3$, 100 MHz): δ 14.8, 18.3, 37.3, 56.3, 118.6, 122.3, 122.7, 123.8, 124.7, 125.1, 125.4, 126.0, 126.4, 128.1, 129.4, 136.0, 137.0, 137.8, 138.1, 138.2, 140.1, 140.2, 144.3, 144.6, 145.2, 146.9, 153.3, 153.4, 155.1. HRMS (ESI) calcd for $C_{67}H_{68}N_2O_4S$ $[M+H]^+$: 997.4978. Found: 997.4961.

Acknowledgments

We are grateful to the National 863 Program (2009AA05Z421) and the Tianjin Natural Science Foundation (09JCZDJC24400) for financial supports.

References

[1] B. O'Regan, M. Grätzel, Nature 353 (1991) 737.
[2] A. Mishra, M.K.R. Fischer, P. Bäuerle, Angew. Chem., Int. Ed. 48 (2009) 2474.
[3] (a) J.E. Benedetti, A.D. Gonçalves, A.L.B. Formiga, M.-A.D. Paoli, X. Li, J.R. Durrant, A.F. Nogueira, J. Power Sources 195 (2010) 1246;
(b) M. Adachi, Y. Murata, J. Takao, J. Jiu, M. Sakamoto, F. Wang, J. Am. Chem. Soc. 126 (2004) 14943;
(c) F. Cai, J. Liang, Z. Tao, J. Chen, R. Xu, J. Power Sources 177 (2008) 631.
[4] Y.-M. Cao, Y. Bai, Q.-J. Yu, Y.-M. Cheng, S. Liu, D. Shi, F.-F. Gao, P. Wang, J. Phys. Chem. C 113 (2009) 6290.
[5] Y.-L. Liang, B. Peng, J. Liang, Z.-L. Tao, J. Chen, Org. Lett. 12 (2010) 1204.
[6] (a) K. Hara, Y. Dan-oh, C. Kasada, Y. Ohga, A. Shinpo, S. Suga, K. Sayama, H. Arakawa, Langmuir 20 (2004) 4205;
(b) Z.S. Wang, Y. Cui, K. Hara, Y. Dan-oh, C. Kasada, A. Shinpo, Adv. Mater. 19 (2007) 1138.
[7] (a) T. Horiuchi, H. Miura, K. Sumioka, S. Uchida, J. Am. Chem. Soc. 126 (2004) 12218;
(b) H.J. Snaith, A. Petrozza, S. Ito, H. Miura, M. Grätzel, Adv. Funct. Mater. 19 (2009) 1810.
[8] (a) J. Pei, S.-J. Peng, J.-F. Shi, Y.-L. Liang, Z.-L. Tao, J. Liang, J. Chen, J. Power Sources 187 (2009) 620;
(b) C.-H Yang, H.-L. Chen, Y.-Y. Chuang, C.-G. Wu, C.-P. Chen, S.-H. Liao, T.-L. Wang, J. Power Sources 188 (2009) 627;
(c) W. Xu, J. Pei, J.-F. Shi, S.-J. Peng, J. Chen, J. Power Sources 183 (2008) 792;
(d) D.P. Hagberg, J.-H. Yum, H. Lee, F.D. Angelis, T. Marinado, K.M. Karlsson, R. Humphry-Baker, L. Sun, A. Hagfeldt, M. Grätzel, M.K. Nazeeruddin, J. Am. Chem. Soc. 130 (2008) 6259;
(e) G. Li, K.-J. Jiang, Y.-F. Li, S.-L. Li, L.-M. Yang, J. Phys. Chem. C 112 (2008) 11591;
(f) Z. Ning, Q. Zhang, W. Wu, H. Pei, B. Liu, H. Tian, J. Org. Chem. 73 (2008) 3791;
(g) A. Baheti, P. Tyagi, K.R.J. Thomas, Y.-C. Hsu, J.T. Lin, J. Phys. Chem. C 113 (2009) 8541;
(h) L. Zhang, Y. Liu, Z. Wang, M. Liang, Z. Sun, S. Xue, Tetrahedron 66 (2010) 3318;
(i) M.-F. Xu, R.-Z. Li, N. Pootrakulchote, D. Shi, J. Guo, Z.-H. Yi, S.M. Zakeeruddin, M. Grätzel, P. Wang, J. Phys. Chem. C 112 (2008) 19770.
[9] (a) K. Hara, M. Kurashige, S. Ito, A. Shinpo, S. Suga, K. Sayama, H. Arakawa, Chem. Commun. (2003) 252;
(b) T. Kitamura, M. Ikeda, K. Shigaki, T. Inoue, N.A. Anderson, X. Ai, T. Lian, S. Yanagida, Chem. Mater. 16 (2004) 1806;
(c) S.-L. Li, K.-J. Jiang, K.-F. Shao, L.-M. Yang, Chem. Commun. (2006) 2792.
[10] (a) S. Kim, J.K. Lee, S.O. Kang, J. Ko, J.-H. Yum, S. Frantacci, F.D. Angelis, D.D. Censo, M.K. Nazeeruddin, M. Grätzel, J. Am. Chem. Soc. 128 (2006) 16701;
(b) H. Choi, C. Baik, S.O. Kang, J. Ko, M.-S. Kang, M.K. Nazeeruddin, M. Grätzel, Angew. Chem., Int. Ed. 47 (2008) 327;
(c) H. Qin, S. Wenger, M. Xu, F. Gao, X. Jing, P. Wang, S.M. Zakeeruddin, M. Grätzel, J. Am. Chem. Soc. 130 (2008) 9202;
(d) H. Choi, J.K. Lee, K. Song, S.O. Kang, J. Ko, Tetrahedron 63 (2007) 3115;
(e) S. Kim, H. Choi, D. Kim, K. Song, S.O. Kang, J. Ko, Tetrahedron 63 (2007) 9206;
(f) S. Kim, H. Choi, C. Baik, K. Song, S.O. Kang, J. Ko, Tetrahedron 63 (2007) 11436.
[11] (a) K. Sayama, K. Hara, N. Mori, M. Satsuki, S. Suga, S. Tsukagoshi, Y. Abe, H. Sugihara, H. Arakawa, Chem. Commun. (2000) 1173;
(b) K. Sayama, S. Tsukagoshi, K. Hara, Y. Ohga, A. Shinpou, Y. Abe, S. Suga, H. Arakawa, J. Phys. Chem. B 106 (2002) 1363.
[12] (a) Z.-S. Wang, F.-Y. Li, C.-H. Huang, Chem. Commun. (2000) 2063;
(b) Q.-H. Yao, L. Shan, F.-Y. Li, D.-D. Yin, C.-H. Huang, New J. Chem. 27 (2003) 1277.
[13] (a) N. Koumura, Z.-S. Wang, S. Mori, M. Miyashita, E. Suzuki, K. Hara, J. Am. Chem. Soc. 128 (2006) 14256;
(b) Z.-S. Wang, N. Koumura, Y. Cui, M. Takahashi, H. Sekiguchi, A. Mori, T. Kubo, A. Furube, K. Hara, Chem. Mater. 20 (2008) 3993.
[14] (a) W.-D. Zeng, Y.-M. Cao, Y. Bai, Y.-H. Wang, Y.-S. Shi, M. Zhang, F.-F. Wang, C.-Y. Pan, P. Wang, Chem. Mater. 22 (2010) 1915;
(b) G. Zhang, H. Bala, Y. Cheng, D. Shi, X. Lv, Q. Yu, P. Wang, Chem. Commun. (2009) 2198.
[15] H. Im, S. Kim, C. Park, S.-H. Jang, C.-J. Kim, K. Kim, N.-G. Park, C. Kim, Chem. Commun. (2010) 1335.
[16] D. Liu, R.W. Fessenden, G.L. Hug, P.V. Kamat, J. Phys. Chem. B 101 (1997) 2583.
[17] Z. Ning, H. Tian, Chem. Commun. (2009) 5483.
[18] (a) D.P. Hagberg, T. Marinado, K.M. Karlsson, K. Nonomura, P. Qin, G. Boschloo, T. Brinck, A. Hagfeldt, L. Sun, J. Org. Chem. 72 (2007) 9550;
(b) W.-H. Liu, I.-C. Wu, C.-H. Lai, C.-H. Lai, P.-T. Chou, Y.-T. Li, C.-L. Chen, Y.-Y. Hsu, Y. Chi, Chem. Commun. (2008) 5152.
[19] X.-Y. Cao, W.-B. Zhang, J.-L. Wang, X.-H. Zhou, H. Lu, J. Pei, J. Am. Chem. Soc. 125 (2003) 12430.
[20] (a) Y. Sun, K. Xiao, Y. Liu, J. Wang, J. Pei, G. Yu, D. Zhu, Adv. Funct. Mater. 15 (2005) 818;
(b) X. Cao, X. Zhou, H. Zi, J. Pei, Macromolecules 37 (2004) 8874.
[21] Z. Ning, Q. Zhang, H. Pei, J. Luan, C. Lu, Y. Cui, H. Tian, J. Phys. Chem. C 113 (2009) 10307.
[22] K.R.J. Thomas, Y.-C. Hsu, J.T. Lin, K.-M. Lee, K.-C. Ho, C.-H. Lai, Y.-M. Cheng, P.-T. Chou, Chem. Mater. 20 (2008) 1830.
[23] A. Hagfeldt, M. Grätzel, Chem. Rev. 95 (1995) 49.
[24] (a) H. Tian, X. Yang, R. Chen, Y. Pan, L. Li, A. Hagfeldt, L. Sun, Chem. Commun. (2007) 3741;
(b) G. Li, Y. Zhou, X. Cao, P. Bao, K. Jiang, Y. Lin, L.-M. Yang, Chem. Commun. (2009) 2201.
[25] Z.-S. Wang, K. Hara, Y. Dan-oh, C. Kasada, A. Shinpo, S. Suga, H. Arakawa, H. Sugihara, J. Phys. Chem. B 109 (2005) 3907.
[26] X.-Y. Cao, W. Zhang, H. Zi, J. Pei, Org. Lett. 26 (2004) 4845.
[27] S. Ito, T.N. Murakami, P. Comte, P. Liska, C. Grätzel, M.K. Nazeeruddin, M. Grätzel, Thin Solid Films 516 (2008) 4613.
[28] M.J. Frisch, G.W. Trucks, H.B. Schlegel, G.E. Scuseria, M.A. Robb, J.R. Cheeseman, J.A. Montgomery Jr., T. Vreven, K.N. Kudin, J.C. Burant, J.M. Millam, S.S. Iyengar, J. Tomasi, V. Barone, B. Mennucci, M. Cossi, G. Scalmani, N. Rega, G.A. Petersson, H. Nakatsuji, M. Hada, M. Ehara, K. Toyota, R. Fukuda, J. Hasegawa, M. Ishida, T. Nakajima, Y. Honda, O. Kitao, H. Nakai, M. Klene, X. Li, J.E. Knox, H.P. Hratchian, J.B. Cross, V. Bakken, C. Adamo, J. Jaramillo, R. Gomperts, R.E. Stratmann, O. Yazyev, A.J. Austin, R. Cammi, C. Pomelli, J.W. Ochterski, P.Y. Ayala, K. Morokuma, G.A. Voth, P. Salvador, J.J. Dannenberg, V.G. Zakrzewski, S. Dapprich, A.D. Daniels, M.C. Strain, O. Farkas, D.K. Malick, A.D. Rabuck, K. Raghavachari, J.B. Foresman, J.V. Ortiz, Q. Cui, A.G. Baboul, S. Clifford, J. Cioslowski, B.B. Stefanov, G. Liu, A. Liashenko, P. Piskorz, I. Komaromi, R.L. Martin, D.J. Fox, T. Keith, M.A. Al-Laham, C.Y. Peng, A. Nanayakkara, M. Challacombe, P.M.W. Gill, B. Johnson, W. Chen, M.W. Wong, C. Gonzalez, J.A. Pople, Gaussian 03, Revision C.02, Gaussian, Inc., Wallingford, CT, 2004.